Atmos. Chem. Phys. Discuss., 14, 6951–6979, 2014
www.atmos-chem-phys-discuss.net/14/6951/2014/
doi:10.5194/acpd-14-6951-2014

Atmospheric Chemistry and Physics Discussions

Improved model of isoprene emissions in Africa using OMI satellite observations of formaldehyde: implications for oxidants and particulate matter

E. A. Marais[1,*], D. J. Jacob[1,2], A. Guenther[3], K. Chance[4], T. P. Kurosu[5], J. G. Murphy[6], C. E. Reeves[7], and H. O. T. Pye[8]

[1]Earth and Planetary Sciences, Harvard University, Cambridge, MA, USA
[2]School of Engineering and Applied Sciences, Harvard University, Cambridge, MA, USA
[3]Pacific Northwest National Laboratory, Richland, WA, USA
[4]Harvard-Smithsonian Center for Astrophysics, Cambridge, MA, USA
[5]Earth Atmosphere Science, Jet Propulsion Laboratory, Pasadena, CA, USA
[6]Department of Chemistry, University of Toronto, Toronto, Canada
[7]School of Environmental Sciences, University of East Anglia, Norwich, UK
[8]National Exposure Research Laboratory, US EPA, Research Triangle Park, NC, USA
[*]now at: School of Engineering and Applied Sciences, Harvard University, Cambridge, MA, USA

Received: 3 February 2014 – Accepted: 28 February 2014 – Published: 14 March 2014

Correspondence to: E. A. Marais (emarais@seas.harvard.edu)

Published by Copernicus Publications on behalf of the European Geosciences Union.

ACPD
14, 6951–6979, 2014

Abstract

We use a 2005–2009 record of isoprene emissions over Africa derived from OMI satellite observations of formaldehyde (HCHO) to better understand the factors controlling isoprene emission on the scale of the continent and evaluate the impact of isoprene emissions on atmospheric composition in Africa. OMI-derived isoprene emissions show large seasonality over savannas driven by temperature and leaf area index (LAI), and much weaker seasonality over equatorial forests driven by temperature. The commonly used MEGAN (version 2.1) global isoprene emission model reproduces this seasonality but is biased high, particularly for equatorial forests, when compared to OMI and relaxed-eddy accumulation measurements. Isoprene emissions in MEGAN are computed as the product of an emission factor E_o, LAI, and activity factors dependent on environmental variables. We use the OMI-derived emissions to provide improved estimates of E_o that are in good agreement with direct leaf measurements from field campaigns (r = 0.55, bias = −19 %). The largest downward corrections to MEGAN E_o values are for equatorial forests and semi-arid environments, and this is consistent with latitudinal transects of isoprene over West Africa from the AMMA aircraft campaign. Total emission of isoprene in Africa is estimated to be 77 Tg C a^{-1}, compared to 104 Tg C a^{-1} in MEGAN. Simulations with the GEOS-Chem oxidant-aerosol model suggest that isoprene emissions increase mean surface ozone in West Africa by up to 8 ppbv, and particulate matter by up to 1.5 µg m^{-3}, due to coupling with anthropogenic influences.

1 Introduction

Isoprene is the dominant biogenic non-methane volatile organic compound (NMVOC) emitted by vegetation, accounting for about 50 % of global NMVOC emissions in current inventories (Olivier et al., 1996; Guenther et al., 2006). Isoprene affects the oxidative capacity of the atmosphere through reaction with OH (Ren et al., 2008; Lelieveld et al.,

ACPD
14, 6951–6979, 2014

2008) and as a precursor of O_3 (Trainer et al., 1987). It is also an important precursor for secondary organic aerosols (SOA) (Claeys et al., 2004) and a temporary reservoir for nitrogen oxide radicals ($NO_x \equiv NO + NO_2$) by formation of organic nitrates (Paulot et al., 2012). Isoprene thus has a range of impacts on air quality and climate that need to be included in atmospheric composition models. The widely used MEGAN global emission model (Guenther et al., 2006, 2012) indicates that 80 % of global isoprene emission takes place in the tropics and 25 % in Africa, but there are large uncertainties in these estimates due to lack of data. In previous work we developed a method to estimate isoprene emissions from Africa on the basis of observations of formaldehyde (HCHO) from the OMI satellite instrument. Here we use our OMI-derived isoprene emissions evaluated with local data to better understand the factors controlling isoprene emissions in Africa, improve emission estimates for different African plant functional types (PFTs), and assess the implications for atmospheric oxidants and aerosols.

Isoprene produced in the chloroplasts of plants is released to the atmosphere via the stomata of leaves (Sharkey and Yeh, 2001). Above-canopy emission fluxes E_{ISOP} depend on plant species, foliage density, leaf age, temperature, photosynthetically active radiation (PAR), and water stress (Guenther et al., 1995). This is commonly represented in isoprene emission models by multiplying an emission factor E_o defined for each PFT at standard conditions with an ensemble of coefficients describing the sensitivity to local environmental variables. In the MEGAN (version 2.1) inventory (Guenther et al., 2012) this is given as

$$E_{ISOP} = E_o \times C_{CE} \times LAI \times \gamma_{PAR} \times \gamma_T \times \gamma_{AGE} \times \gamma_{SM}. \quad (1)$$

where LAI is the leaf area index (m^2 leaf surface m^{-2} of Earth surface) and the dimensionless activity factors γ describe the sensitivity to above-canopy radiation (PAR), air temperature (T), leaf age distribution (AGE), and soil moisture (SM). The coefficient C_{CE} (m^2 Earth surface m^{-2} leaf surface) enforces $E_{ISOP} = E_o$ under standard conditions, which for MEGAN are defined as $T = 303$ K and PAR = 1000 µmol photons m^{-2} s^{-1}, and a canopy with LAI = 5 m^2 m^{-2}, leaf age distribution of

ACPD
14, 6951–6979, 2014

80 % mature, 10 % growing, and 10 % senescing leaves, and volumetric soil moisture of 0.3 $m^3 m^{-3}$. The value of C_{CE} depends on the radiative transfer model used to describe the attenuation of PAR by the canopy.

Isoprene emission data for African vegetation are very limited, and emission models require extrapolation of data from other continents and across plant species (Guenther et al., 2006, 2012). This can lead to substantial errors, as differences in isoprene fluxes within and across plant species are large. Uncertainty in the distribution of land cover (PFT) in the tropics can further lead to a 5-fold discrepancy in isoprene emissions in equatorial Africa (Pfister et al., 2008).

Space-based observations of HCHO, a high-yield oxidation product of isoprene, have been used in a number of studies to infer isoprene emissions and evaluate inventories globally (Shim et al., 2005; Stavrakou et al., 2009a, b) and regionally in Southeast Asia (Fu et al., 2007), South America (Barkley et al., 2008), North America (Palmer et al., 2003, 2006; Millet et al., 2008), Europe (Dufour et al., 2009; Curci et al., 2010), and Africa (Marais et al., 2012). These studies have confirmed temperature as the dominant factor controlling month-to-month variability of isoprene emissions across North America (Palmer et al., 2006; Millet et al., 2008) and Amazonia (Barkley et al., 2008). Leaf phenology and PAR were found to be additional important drivers of isoprene emission seasonality in Amazonia (Barkley et al., 2008, 2009). Stavrakou et al. (2009a) found that water stress reduces isoprene emissions in southern Africa during the dry season. Here we use our previous work for Africa (Marais et al., 2012) to better understand the factors controlling isoprene emissions across the African continent and evaluate and improve the MEGANv2.1 emission inventory.

2 OMI-derived isoprene emissions in Africa

The derivation of isoprene emissions in Africa using OMI HCHO data is described in Marais et al. (2012) and summarized briefly here. OMI is a UV/VIS solar backscatter instrument on the Aura polar sun-synchronous satellite launched in 2004 (Levelt et al.,

ACPD
14, 6951–6979, 2014

2006). It has a 13 km × 24 km nadir pixel resolution, daily global coverage through cross-track viewing, and 13:30 local time (LT) overpass. HCHO slant columns are obtained from version 2.0 (Collection 3) retrievals for 2005–2009 (http://disc.sci.gsfc.nasa.gov/Aura/data-holdings/OMI/omhcho_v003.shtml). They are corrected for instrument drift and converted to vertical columns using local air mass factors (AMF) for the scattering atmosphere (Palmer et al., 2001) with vertical HCHO profiles from the GEOS-Chem chemical transport model v9-01-03 (http://www.geos-chem.org) and scattering weights from the LIDORT radiative transfer model (Spurr et al., 2001).

HCHO enhancements over Africa primarily originate from isoprene emission, biomass burning, and fuel combustion. Scenes affected by biomass burning are excluded on the basis of MODIS satellite observations of fire counts and OMI satellite observations of aerosol absorption optical depth (AAOD) (Torres et al., 2007). Scenes affected by gas flaring are excluded on the basis of a specialized hotspot product from the AATSR satellite sensor (Casadio et al., 2012) and this leads to the exclusion of much of Nigeria where that source is particularly large and urban and industrial sources may contribute as well (Marais et al., 2014).

Marais et al. (2012) thus obtained a 2005–2009 monthly data set of vertical HCHO columns with 1° × 1° spatial resolution screened for biomass burning and anthropogenic influences and thus attributable to isoprene emissions (Fig. 1, left panel). They used GEOS-Chem to derived the sensitivity, S, of column HCHO Ω_{HCHO} to a perturbation Δ in isoprene emission E_{ISOP} ($S = \Delta\Omega_{HCHO}/\Delta E_{ISOP}$). Values of S are sensitive to NO_x concentrations and this was accounted for using concurrent observations of OMI tropospheric NO_2 columns. Scenes affected by smearing (displacement of HCHO from the isoprene emission source) were diagnosed with anomalously high values of S and excluded from the data set.

Marais et al. (2012) obtained in this manner a monthly isoprene emission inventory for 2005–2009 on a 1° × 1° grid (Fig. 1, center panel). The OMI overpass is at 13:30 LT and the corresponding isoprene emissions are for 12:00–15:00 LT, typically the diurnal maximum. Also shown in Fig. 1 is the MODIS IGBP land cover map (Friedl et al.,

ACPD
14, 6951–6979, 2014

2002). Dominant vegetation types in Africa are roughly defined by latitudinal bands, with evergreen (broadleaf) trees along the Equator successively transitioning to the north and south to woody savannas (30–60 % tree coverage), savannas (10–30 %), grasslands, and deserts. The HCHO column data follow this vegetation gradient and so too do the inferred isoprene emissions.

Marais et al. (2012) presented a detailed error characterization of their OMI-derived isoprene emissions. Spectral fitting of the HCHO column has an error standard deviation of 8×10^{15} molecules cm^{-2} for individual observations. Relating the fitted slant HCHO columns to isoprene emissions incurs errors in the AMF estimate (20 %), the isoprene oxidation mechanism (15 %), the use of OMI NO_2 to obtain S under low-NO_x conditions (20–40 %), and smearing (30 % for high-NO_x conditions, 30–70 % for low-NO_x). The resulting error in isoprene emission estimates for individual scenes, adding in quadrature all error contributions, is 40 % for high-NO_x conditions and 40–90 % for low-NO_x (Marais et al., 2012). A monthly mean estimate for a $1^\circ \times 1^\circ$ gridsquare typically averages 3000 individual scenes. Averaging reduces the error though only to the extent that the error components are random.

3 Evaluation with canopy flux measurements

Canopy-scale isoprene flux measurements by relaxed-eddy accumulation (REA) are available from a few African field campaigns. Figure 2 compares OMI-derived isoprene emissions to REA measurements over equatorial evergreen trees (Greenberg et al., 1999; Serça et al., 2001), woody savannas (Greenberg et al., 1999), and savannas (Harley et al., 2003) in central and southern Africa (sites 1–4 in Fig. 1). Also shown are the values calculated using Eq. (1) with MEGAN v2.1 emission factors, combined Terra and Aqua MODIS LAI (Yang et al., 2006), and the Goddard Earth Observing System (GEOS-5) assimilated meteorological data. The Serça et al. (2001) and Harley et al. (2003) measurements (sites 1 and 4) are from walk-up towers with a flux footprint of about 600 m, while the Greenberg et al. (1999) measurements (sites 2 and 3) are

ACPD
14, 6951–6979, 2014

from aircraft with a flux footprint of ∼ 100 km × 100 km at site 2 and 30 km × 30 km at site 3. All values in Fig. 2 are for 12:00–15:00 LT. REA fluxes at sites 2–3, obtained in the morning (09:30–11:30 LT), are increased by a factor of 1.4 as a diurnal correction for temperature and PAR following MEGAN.

OMI and MEGAN are sampled for the 1° × 1° gridsquare coincident with the observation site and for the corresponding months. Interannual variability is of similar magnitude in the OMI-derived and MEGAN data at sites 1 (November), 2 and, 3 where multi-year OMI data are available. The variability is driven in MEGAN predominantly by temperature. At site 3 there are no OMI data in the months of observation (November–December) because of biomass burning interference and we show instead OMI-derived emissions in September–October, which should be similar to November–December according to MEGAN.

For the equatorial evergreen tree sites in central Africa (sites 1 and 2) OMI-derived isoprene emissions are on average 2 times higher than the REA measurements and MEGAN is 5 times higher. The flux tower sampled vegetation with a relatively low fraction of isoprene emitters. Nearby landscapes include monodominant stands of the *Gilbertiodendron* trees that have a high isoprene emission factor (Serça et al., 2001). The distribution of this tree species beyond the sampling domain is uncertain and application of its emission factor to land cover in equatorial Africa contributes to the overestimate in MEGAN. OMI and MEGAN reproduce the March–November decline at site 1 and this is driven in MEGAN by temperature.

Fluxes at site 2, where the sampling footprint is similar to OMI, have large spatial variability implying that differences in the sampling footprint contribute to discrepancies. Greenberg et al. (1999) applied a positive correction of ∼ 20 % to flux measurements at sites 2–3 to account for the transport of isoprene that was not accumulated in the two REA reservoirs. A similar negative bias may affect measurements at sites 1 and 4 but the reported values have not been adjusted. An additional negative bias associated with the aircraft REA measurements (sites 2 and 3), but not with the tower sites (1 and 4), is the vertical flux divergence between the height of the aircraft measurement

ACPD
14, 6951–6979, 2014

and the surface flux. The isoprene vertical flux divergence profiles investigated by Karl et al. (2013) suggest that the fluxes reported by Greenberg et al. (1999) should be increased by a further 25 %.

At the woody savanna site OMI is 2.2 times higher than the REA measurement (1.8 times higher if a 25 % upward correction is applied to the REA measurement), while MEGAN is 8 times higher. At the savanna site OMI is 1.3 times higher than the REA flux measurement while MEGAN is 2.4 times higher. The discrepancy at site 4 is partly due to the low (< 10 %) proportion of isoprene emitting vegetation within the flux tower footprint as compared to ∼ 35 % for savannas surveyed at surrounding field sites (Harley et al., 2003).

Overall the REA flux measurements indicate canopy-scale isoprene emissions that are somewhat lower than derived from OMI and much lower than derived from MEGAN. As we will show in Sect. 5, isoprene emission factors obtained with OMI are more consistent with landscape-level field campaign measurements and lead to an improved estimate of isoprene emissions from MEGAN.

4 Seasonality of isoprene emissions in Africa

We examine the seasonality of our OMI-derived isoprene emissions in relation to environmental variables, focusing on three seasonally and ecologically coherent regions in Africa where emissions are highest (Fig. 3): (1) equatorial forests dominated by tropical broadleaf evergreen trees, (2) northern savannas (including woody), and (3) southern savannas (including woody). Figure 4 shows the seasonality of OMI-derived isoprene emissions for these three regions together with MODIS LAI and GEOS-5 2 m air temperature. Isoprene emissions and 2 m temperature are for 12:00–15:00 LT and MODIS LAI is the combined Terra and Aqua product (Yang et al., 2006). Multi-year averages (2005–2009) are shown as the regionally averaged interannual variability is small, except over northern savannas in August as discussed below.

ACPD
14, 6951–6979, 2014

OMI-derived isoprene emissions for equatorial forests are a factor of 2 lower than MEGAN and both show similar weak seasonality, with a decline from March to November that is consistent with the Serça et al. (2001) REA flux measurements (Fig. 2) and is driven in MEGAN principally by temperature. Although LAI exhibits similar seasonality, it remains above 3.5 $m^2 m^{-2}$ year-round and MEGAN is not sensitive to LAI values above 2–3 $m^2 m^{-2}$ due to shading of lower-canopy leaves (Guenther et al., 2006).

Availability of OMI-derived isoprene emission data for the northern savannas is limited to April–November because of pervasive biomass burning influence during the December–March dry season. Emissions are maximum in April, at the beginning of the wet season, and minimum in August when the West African Monsoon (WAM) is fully developed over the continent (Janicot et al., 2008) resulting in cooler temperatures. OMI-derived emissions largely follow temperature over the April–November period. Year-to-year variability in the WAM affects temperature in August, leading to interannual variability in August OMI isoprene emissions over the 2005–2009 period that is correlated with temperature ($r = 0.55$).

The complete seasonality simulated by MEGAN in northern savannas shows low isoprene emissions in the December–March dry season when LAI is less than 1 $m^2 m^{-2}$, and a broad maximum in the April–November wet season as the August minimum in temperature is compensated by a corresponding maximum in LAI. MODIS LAI in the northern savannas is less than 2.5 $m^2 m^{-2}$ year-round, sufficiently low that the MEGAN dependence on LAI does not saturate (Guenther et al., 2012). However, MODIS may underestimate LAI in West Africa during the wet season because of cloud contamination (Gessner et al., 2013).

OMI-derived emissions for southern savannas are in close agreement with MEGAN, featuring a minimum in the winter dry season and a maximum in the summer wet season. The seasonal minimum follows that of temperature (June–July) with a 1 month lag that reflects the very dry conditions in July–September. We find that LAI and temperature are both important for driving the seasonality of isoprene emissions in southern savannas.

ACPD
14, 6951–6979, 2014

5 Satellite-derived isoprene emission factors for Africa

The general ability of MEGAN to reproduce the seasonal variation of OMI-derived isoprene emissions suggests that the MEGAN activity factors (γ in Eq. 1) are appropriate for conditions in Africa, with temperature and LAI as the principal drivers. The large MEGAN bias over equatorial forests and northern savannas can therefore be attributed to an overestimate of emission factors (E_o in Eq. 1) that results from uncertainties in PFT distribution and limited emission data for plant species in these regions.

The emission factors in MEGAN are isoprene fluxes for a canopy with leaves at standard conditions of air temperature ($T = 303\,\mathrm{K}$) and light (PAR = $1000\,\mu\mathrm{mol\,photons\,m^{-2}\,s^{-1}}$) gridded to a detailed regional land cover map for Africa south of the Equator (Otter et al., 2003) and the Olson et al. (2001) global ecoregion data in the north (Guenther et al., 2006). We can infer them from the OMI-derived canopy-level isoprene emission data by using Eq. (1). In so doing we only consider individual activity factors γ within the range 0.5–1.5.

Figure 5 shows the resulting distributions of MEGAN and OMI emission factors E_o over Africa together with observations from field campaigns. The latter are at the landscape-level and were obtained by scaling measured leaf-level isoprene fluxes for representative plant species with foliage density and species distribution data. Leaf-level measurements at standard conditions were obtained by using enclosure measurements with controlled temperature and PAR (Otter et al., 2002; Serça et al., 2001), or adjusting to standard conditions with MEGAN activity factors for temperature and PAR (Guenther et al., 1996). For the former an upward correction applied to the Serça et al. (2001) landscape emission factor accounts for isoprene fluxes obtained from shade-adapted leaves that have lower emissions at standard conditions than sunlit leaves (Guenther et al., 1999). Leaf-level fluxes of Klinger et al. (1998) were determined to be at standard conditions with coincident measurements of temperature and PAR, but we exclude the data from shaded leaves at dense forest sites.

ACPD
14, 6951–6979, 2014

We find from Fig. 5 remarkable agreement between OMI-derived emission factors and the field data (r = 0.55, OMI normalized mean bias = −19 %). Woody savannas in Zambia and savannas in South Africa have large variability in E_o (0.5–4.5 mg C m^{-2} h^{-1}) that is reproduced by OMI. The two sites in Botswana have low emission factors as the site to the north is dominated by monoterpene emitting mopane vegetation, while the site to the south is predominantly shrubland (Otter et al., 2002).

Differences between OMI and MEGAN emission factors are largest for equatorial forests, and the field enclosure observations are in good agreement with OMI and much lower than MEGAN. The equatorial forest enclosure measurements are used in MEGAN to estimate emission factors there, but a large positive correction is applied to account for leaf enclosure measurements of shade-adapted leaves. Our OMI-derived emission factors do not support a large positive correction, and this is also reflected in the MEGAN overestimate of REA flux measurements (Fig. 2). OMI emission factors for equatorial forests are larger in the west than east and this may result from differences in the proportion of isoprene emitting species. The west is dominated by dry tropical forests, while the east is dominated by permanently or seasonally flooded forests (White, 1983).

Table 1 shows mean isoprene emission factors for individual PFTs as obtained by mapping the data from Fig. 5 onto the MODIS IGBP land map (Friedl et al., 2002) and the Global Land Cover (GLC) 2000 land map (Mayaux et al., 2006). The distribution of MODIS IGBP woody savannas is spatially consistent with GLC 2000 broadleaf trees and MODIS IGBP savannas correspond to GLC 2000 shrubs interspersed with broadleaf trees and cultivated land. The GLC 2000 classification scheme is more consistent with the PFTs of MEGANv2.1 (Guenther et al., 2012). OMI gives higher emission factors for forested vegetation than for grasslands but the difference is not as large as MEGAN and more consistent with the field enclosure observations. The largest differences between OMI and MEGAN emission factors are for broadleaf evergreen trees and for semi-arid vegetation (shrubs and herbs).

ACPD
14, 6951–6979, 2014

The OMI-derived emission factors in Fig. 5 can be used to improve the MEGAN isoprene emission estimates as computed from Eq. (1). Figure 6 compares the resulting isoprene concentrations simulated by GEOS-Chem with a latitudinal profile of isoprene concentration measurements below 1 km across West Africa during the AMMA wet season aircraft campaign in July–August 2006 (Murphy et al., 2010). There is a strong vegetation gradient along the AMMA flight track from the Gulf of Guinea to Benin woodlands to arid conditions in the north that is reflected in the isoprene data. Simulated isoprene in GEOS-Chem is a factor of 2 too low over Benin woodlands likely due to a seasonal low bias in MODIS LAI over West Africa from cloud contamination (Gessner et al., 2013). Isoprene emissions over the AMMA domain are not only sensitive to LAI, but also MEGAN emission factors (Ferreira et al., 2010). The OMI-derived emission factors are much better able to reproduce the latitudinal gradient than the original MEGAN emission factors, including in particular the decline to the north associated with increased aridity. Throughout Africa MEGAN emission factors are too high for semi-arid PFTs, as indicated by the overestimate in MEGAN for GLC 2000 sparse herb/shrub cover in Table 1.

6 Implications for oxidants and aerosols

We use the GEOS-Chem chemical transport model to (1) evaluate the change in atmospheric composition that results from replacing MEGAN emission factors with those obtained using OMI, and (2) determine the impact of isoprene emissions using OMI-derived emission factors on aerosols and oxidants. GEOS-Chem includes the standard representation of oxidant-aerosol chemistry as described for example by Mao et al. (2010) with updates to the isoprene oxidation mechanism (Paulot et al., 2009a, b).

Total annual isoprene emissions in Africa averaged over 2005–2009 using OMI-derived emission factors are 77 $\mathrm{Tg\,C\,a^{-1}}$, as compared to 104 $\mathrm{Tg\,C\,a^{-1}}$ in MEGAN v2.1. The difference is mainly for the equatorial evergreen forest PFT in central Africa, where

ACPD
14, 6951–6979, 2014

OMI-derived isoprene emissions are 2–3 times lower than MEGAN. GEOS-Chem using OMI-derived isoprene emissions indicates a factor of 4 increase in boundary layer OH concentrations over central Africa relative to MEGAN, a 4 ppbv increase in surface O_3, and 8 ppbv decrease in surface isoprene.

Figure 7 shows the effect of African isoprene emissions on surface concentrations of daily maximum 8 h average (MDA8) O_3, particulate matter (PM), NO_x, and OH. We calculated this effect by difference between a GEOS-Chem simulation with OMI-derived isoprene emission factors and a simulation with no isoprene emission. The largest effect on O_3 is over West Africa because of high anthropogenic, soil, and biomass burning NO_x emissions (Marais et al., 2014). The largest effect on PM is also over West Africa and reflects the availability of high pre-existing primary PM from combustion (biomass burning and fuel) on which isoprene oxidation products can condense. NO_x declines in West Africa and the tropics due to formation of isoprene nitrates. Loss of OH from reaction with isoprene is highest in the tropics where low levels of NO_x limit the recycling of HO_x radicals.

7 Conclusions

We used a 2005–2009 data set of monthly isoprene emissions in Africa derived from OMI satellite observations of formaldehyde (HCHO) to study the factors controlling these emissions in different areas of the continent. Our goal was to achieve a better representation of isoprene emission in chemical transport models (CTMs), in part through evaluation and improvement of the commonly used MEGAN emission inventory, and to examine the implications for oxidants and aerosols over the continent.

We began by evaluating the OMI-derived isoprene emissions with relaxed-eddy accumulation flux (REA) measurements obtained from above-canopy towers and aircraft during African field campaigns. OMI-derived isoprene emissions are on average 2 times higher than REA measurements over the equatorial forest and woody savan-

ACPD
14, 6951–6979, 2014

nas but this could reflect biases in the measurements. MEGAN emissions are 5–10 times higher.

We subdivided Africa into 3 seasonally and ecologically coherent regions to examine the seasonality in OMI-derived isoprene emissions, and compare to the seasonality in MEGAN and in driving environmental variables. Equatorial forests exhibit weak seasonality that is driven predominantly by temperature, while seasonality in savannas is driven by both temperature and LAI, in a manner consistent with MEGAN.

Isoprene emissions in MEGAN are computed as the product of (1) an emission factor E_o characteristic of the PFT, (2) the LAI, and (3) activity factors dependent on local environmental variables. We applied the LAI and MEGAN activity factors to our OMI-derived isoprene emissions to obtain emission factors representative of different PFTs. These agree well with the ensemble of leaf-level flux measurements in Africa and imply large downward corrections to MEGAN emission factors for equatorial forests and semi-arid vegetation. Such corrections are consistent with the latitudinal gradient of isoprene across West Africa measured in the AMMA field campaign.

The OMI-derived emission factors can be incorporated into the MEGAN formalism (Eq. 1) to improve modeling of isoprene emissions in Africa. The resulting isoprene emissions for the continent are $77\,\mathrm{Tg\,C\,a^{-1}}$, as compared to $104\,\mathrm{Tg\,C\,a^{-1}}$ in the standard MEGAN inventory. Most of the difference is over equatorial Africa. We conducted GEOS-Chem simulations with and without African isoprene emissions (using OMI-derived emission factors) to examine the impact on regional particulate matter (PM) and oxidants. The largest effect of isoprene emissions on surface O_3 is over West Africa where NO_x is high, and the largest effect on PM is also over West Africa because of pre-existing high concentrations of primary PM from combustion.

Acknowledgements. This work was funded by NASA through the Aura Science Team and by a South African National Research Scholarship for Study Abroad awarded to E. A. Marais. The United States Environmental Protection Agency through its Office of Research and Development collaborated in the research described here. It has been subjected to Agency review and approved for publication, but may not necessarily reflect official Agency policy.

ACPD
14, 6951–6979, 2014

References

Barkley, M. P., Palmer, P. I., Kuhn, U., Kesselmeier, J., Chance, K., Kurosu, T. P., Martin, R. V., Helmig, D., and Guenther, A.: Net ecosystem fluxes of isoprene over tropical South America inferred from Global Ozone Monitoring Experiment (GOME) observations of HCHO columns, J. Geophys. Res., 113, D20304, doi:10.1029/2008JD009863, 2008.

Barkley, M. P., Palmer, P. I., De Smedt, I., Karl, T., Guenther, A., and Van Roozendael, M.: Regulated large-scale annual shutdown of Amazonian isoprene emissions?, Geophys. Res. Lett., 36, L04803, doi:10.1029/2008GL036843, 2009.

Casadio, S., Arino, O., and Serpe, D.: Gas flaring monitoring from space using the ATSR instrument series, Remote Sens. Environ., 116, 239–249, doi:10.1016/j.rse.2010.11.022, 2012.

Claeys, M., Graham, B., Vas, G., Wang, W., Vermeylen, R., Pashynska, V., Cafmeyer, J., Guyon, P., Andreae, M. O., Artaxo, P., and Maenhaut, W.: Formation of secondary organic aerosols through photooxidation of isoprene, Science, 303, 1173–1176, doi:10.1126/science.1092805, 2004.

Curci, G., Palmer, P. I., Kurosu, T. P., Chance, K., and Visconti, G.: Estimating European volatile organic compound emissions using satellite observations of formaldehyde from the Ozone Monitoring Instrument, Atmos. Chem. Phys., 10, 11501–11517, doi:10.5194/acp-10-11501-2010, 2010.

Dufour, G., Wittrock, F., Camredon, M., Beekmann, M., Richter, A., Aumont, B., and Burrows, J. P.: SCIAMACHY formaldehyde observations: constraint for isoprene emission estimates over Europe?, Atmos. Chem. Phys., 9, 1647–1664, doi:10.5194/acp-9-1647-2009, 2009.

Ferreira, J., Reeves, C. E., Murphy, J. G., Garcia-Carreras, L., Parker, D. J., and Oram, D. E.: Isoprene emissions modelling for West Africa: MEGAN model evaluation and sensitivity analysis, Atmos. Chem. Phys., 10, 8453–8467, doi:10.5194/acp-10-8453-2010, 2010.

Friedl, M. A., McIver, D. K., Hodges, J. C. F., Zhang, X. Y., Muchoney, D., Strahler, A. H., Woodcock, C. E., Gopal, S., Schneider, A., Cooper, A., Baccini, A., Gao, F., and Schaaf, C.: Global land cover mapping from MODIS: algorithms and early results, Remote Sens. Environ., 83, 287–302, 2002.

Fu, T.-M., Jacob, D. J., Palmer, P. I., Chance, K., Wang, Y. X., Barletta, B., Blake, D. R., Stanton, J. C., and Pilling, M. J.: Space-based formaldehyde measurements as constraints on

ACPD
14, 6951–6979, 2014

volatile organic compound emissions in east and south Asia and implications for ozone, J. Geophys. Res., 112, D06312, doi:10.1029/2006JD007853, 2007.
Gessner, U., Niklaus, M., Kuenzer, C., and Dech, S.: Intercomparison of leaf area index products for a gradient of sub-humid to arid environments in West Africa, Remote Sens., 5, 1235–1257, doi:10.3390/rs5031235, 2013.
Greenberg, J. P., Guenther, A. B., Madronich, S., Baugh, W., Ginoux, P., Druilhet, A., Delmas, R., and Delon, C.: Biogenic volatile organic compound emissions in central Africa during the Experiment for the Regional Sources and Sinks of Oxidants (EXPRESSO) biomass burning season, J. Geophys. Res., 104, 30659–30671, doi:10.1029/1999JD900475, 1999.
Guenther, A., Hewitt, C. N., Erickson, D., Fall, R., Geron, C., Graedel, T., Harley, P., Klinger, L., Lerdau, M., McKay, W. A., Pierce, T., Scholes, B., Steinbrecher, R., Tallamraju, R., Taylor, J., and Zimmerman, P.: A global model of natural volatile organic compound emissions, J. Geophys. Res., 100, 8873–8892, doi:10.1029/94JD02950, 1995.
Guenther, A., Otter, L., Zimmerman, P., Greenberg, J., Scholes, R., and Scholes, M.: Biogenic hydrocarbon emissions from southern African savannas, J. Geophys. Res., 101, 25859–25865, doi:10.1029/96JD02597, 1996.
Guenther, A., Baugh, B., Brasseur, G., Greenberg, J., Harley, P., Klinger, L., Serça, D., and Vierling, L.: Isoprene emission estimates and uncertainties for the Central African EXPRESSO study domain, J. Geophys. Res., 104, 30625–30639, doi:10.1029/1999JD900391, 1999.
Guenther, A., Karl, T., Harley, P., Wiedinmyer, C., Palmer, P. I., and Geron, C.: Estimates of global terrestrial isoprene emissions using MEGAN (Model of Emissions of Gases and Aerosols from Nature), Atmos. Chem. Phys., 6, 3181–3210, doi:10.5194/acp-6-3181-2006, 2006.
Guenther, A. B., Jiang, X., Heald, C. L., Sakulyanontvittaya, T., Duhl, T., Emmons, L. K., and Wang, X.: The Model of Emissions of Gases and Aerosols from Nature version 2.1 (MEGAN2.1): an extended and updated framework for modeling biogenic emissions, Geosci. Model Dev., 5, 1471–1492, doi:10.5194/gmd-5-1471-2012, 2012.
Harley, P., Otter, L., Guenther, A., and Greenberg, J.: Micrometeorological and leaf-level measurements of isoprene emissions from a southern African savanna, J. Geophys. Res., 108, 8468, doi:10.1029/2002JD002592, 2003.
Janicot, S., Thorncroft, C. D., Ali, A., Asencio, N., Berry, G., Bock, O., Bourles, B., Caniaux, G., Chauvin, F., Deme, A., Kergoat, L., Lafore, J.-P., Lavaysse, C., Lebel, T., Marticorena, B., Mounier, F., Nedelec, P., Redelsperger, J.-L., Ravegnani, F., Reeves, C. E., Roca, R., de Ros-

ACPD
14, 6951–6979, 2014

nay, P., Schlager, H., Sultan, B., Tomasini, M., Ulanovsky, A., and ACMAD forecasters team: Large-scale overview of the summer monsoon over West Africa during the AMMA field experiment in 2006, Ann. Geophys., 26, 2569–2595, doi:10.5194/angeo-26-2569-2008, 2008.

Karl, T., Misztal, P. K., Jonsson, H. H., Shertz, S., Goldstein, A. H., and Guenther, A. B.: Airborne flux measurements of BVOCs above Californian oak forests: experimental investigation of surface and entrainment fluxes, OH densities and Dahmköhler numbers, J. Atmos. Sci., 70, 3277–3287, 2013.

Klinger, L. F., Greenberg, J., Guenther, A., Tyndall, G., Zimmerman, P., M'Bangui, M., Moutsamboté, J.-M., and Kenfack, D.: Patterns in volatile organic compound emissions along a savanna-rainforest gradient in central Africa, J. Geophys. Res., 103, 1443–1454, doi:10.1029/97JD02928, 1998.

Lelieveld, J., Butler, T. M., Crowley, J. N., Dillon, T. J., Fischer, H., Ganzeveld, L., Harder, H., Lawrence, M. G., Martinez, M., Taraborrelli, D., and Williams, J.: Atmospheric oxidation capacity sustained by a tropical forest, Nature, 452, 737–740, doi:10.1038/nature06870, 2008.

Levelt, P. F., van den Oord, G. H. J., Dobber, M. R., Mälkki, A., Visser, H., de Vries, J., Stammes, P., Lundell, J. O. V., and Saari, H.: The Ozone Monitoring Instrument, IEEE T. Geosci. Remote, 44, 1093–1101, doi:10.1109/TGRS.2006.872333, 2006.

Mao, J., Jacob, D. J., Evans, M. J., Olson, J. R., Ren, X., Brune, W. H., Clair, J. M. St., Crounse, J. D., Spencer, K. M., Beaver, M. R., Wennberg, P. O., Cubison, M. J., Jimenez, J. L., Fried, A., Weibring, P., Walega, J. G., Hall, S. R., Weinheimer, A. J., Cohen, R. C., Chen, G., Crawford, J. H., McNaughton, C., Clarke, A. D., Jaeglé, L., Fisher, J. A., Yantosca, R. M., Le Sager, P., and Carouge, C.: Chemistry of hydrogen oxide radicals (HO_x) in the Arctic troposphere in spring, Atmos. Chem. Phys., 10, 5823–5838, doi:10.5194/acp-10-5823-2010, 2010.

Marais, E. A., Jacob, D. J., Kurosu, T. P., Chance, K., Murphy, J. G., Reeves, C., Mills, G., Casadio, S., Millet, D. B., Barkley, M. P., Paulot, F., and Mao, J.: Isoprene emissions in Africa inferred from OMI observations of formaldehyde columns, Atmos. Chem. Phys., 12, 6219–6235, doi:10.5194/acp-12-6219-2012, 2012.

Marais, E. A., Jacob, D. J., Wecht, K., Lerot, C., Kurosu, T. P., and Chance, K.: Anthropogenic emissions in Nigeria and air quality implications: a view from space, Atmos. Environ., in review, 2014.

Mayaux, P., Eva, H., Gallego, J., Strahler, A. H., Herold, M., Agrawal, S., Naumov, S., De Miranda, E. E., Di Bella, C. M., Ordoyne, C., Kopin, Y., and Roy, P. S.: Valida-

ACPD
14, 6951–6979, 2014

tion of the Global Land Cover 2000 map, IEEE T. Geosci. Remote, 44, 1728–1739, doi:10.1109/TGRS.2006.864370, 2006.

Millet, D. B., Jacob, D. J., Boersma, K. F., Fu, T.-M., Kurosu, T. P., Chance, K., Heald, C. L., and Guenther, A.: Spatial distribution of isoprene emissions from North America derived from formaldehyde column measurements by the OMI satellite sensor, J. Geophys. Res., 113, D02307, doi:10.1029/2007JD008950, 2008.

Murphy, J. G., Oram, D. E., and Reeves, C. E.: Measurements of volatile organic compounds over West Africa, Atmos. Chem. Phys., 10, 5281–5294, doi:10.5194/acp-10-5281-2010, 2010.

Olivier, J. G. J., Bouwman, A. F., van der Maas, C. W. M., Berdowski, J. J. M., Veldt, C., Bloos, J. P. J., Visschedijk, A. J. H., Zandveld, P. Y. J., and Haverlag, J. L.: Description of EDGAR Version 2.0: A Set of Global Emission Inventories of Greenhouse Gases and Ozone-Depleting Substances for All Anthropogenic and Most Natural Sources on a Per Country Basis and on 1° × 1° Grid, RIVM, Bilthoven, the Netherlands, 1996.

Olson, D. M., Dinerstein, E., Wikramanayake, E. D., Burgess, N. D., Powell, G. V. N., Underwood, E. C., D'Amico, J. A., Itoua, I., Strand, H. E., Morrison, J. C., Loucks, C. J., Allnutt, T. F., Rickets, T. H., Kura, Y., Lamoreux, J. F., Wettengel, W. W., Hedao, P., and Kassem, K. R.: Terrestrial ecoregions of the world: a new map of life on earth, Bioscience, 51, 933–938, 2001.

Otter, L. B., Guenther, A., and Greenberg, J.: Seasonal and spatial variations in biogenic hydrocarbon emissions from southern African savannas and woodlands, Atmos. Environ., 36, 4265–4275, 2002.

Otter, L., Guenther, A., Wiedinmyer, C., Fleming, G., Harley, P., and Greenberg, J.: Spatial and temporal variations in biogenic volatile organic compound emissions for Africa south of the equator, J. Geophys. Res., 108, 8505, doi:10.1029/2002JD002609, 2003.

Palmer, P. I., Jacob, D. J., Chance, K., Martin, R. V., Spurr, R. J. D., Kurosu, T. P., Bey, I., Yantosca, R., Fiore, A., and Li, Q.: Air mass factor formulation for spectroscopic measurements from satellites: application to formaldehyde retrievals from the Global Ozone Monitoring Experiment, J. Geophys. Res., 106, 14539–14550, doi:10.1029/2000JD900772, 2001.

Palmer, P. I., Jacob, D. J., Fiore, A. M., Martin, R. V., Chance, K., and Kurosu, T. P.: Mapping isoprene emissions over North America using formaldehyde column observations from space, J. Geophys. Res., 108, 4180, doi:10.1029/2002JD002153, 2003.

ACPD
14, 6951–6979, 2014

Palmer, P. I., Abbot, D. S., Fu, T.-M., Jacob, D. J., Chance, K., Kurosu, T. P., Guenther, A., Wiedinmyer, C., Stanton, J. C., Pilling, M. J., Pressley, S. N., Lamb, B., and Sumner, A. L.: Quantifying the seasonal and interannual variability of North American isoprene emissions using satellite observations of the formaldehyde column, J. Geophys. Res., 111, D12315, doi:10.1029/2005JD006689, 2006.

Paulot, F., Crounse, J. D., Kjaergaard, H. G., Kroll, J. H., Seinfeld, J. H., and Wennberg, P. O.: Isoprene photooxidation: new insights into the production of acids and organic nitrates, Atmos. Chem. Phys., 9, 1479–1501, doi:10.5194/acp-9-1479-2009, 2009a.

Paulot, F., Crounse, J. D., Kjaergaard, H. G., Kürten, A., St Clair, J. M., Seinfeld, J. H., and Wennberg, P. O.: Unexpected epoxide formation in the gas-phase photooxidation of isoprene, Science, 325, 730–733, doi:10.1126/science.1172910, 2009b.

Paulot, F., Henze, D. K., and Wennberg, P. O.: Impact of the isoprene photochemical cascade on tropical ozone, Atmos. Chem. Phys., 12, 1307–1325, doi:10.5194/acp-12-1307-2012, 2012.

Pfister, G. G., Emmons, L. K., Hess, P. G., Lamarque, J.-F., Orlando, J. J., Walters, S., Guenther, A., Palmer, P. I., and Lawrence, P. J.: Contribution of isoprene to chemical budgets: a model tracer study with the NCAR CTM MOZART-4, J. Geophys. Res., 113, D05308, doi:10.1029/2007JD008948, 2008.

Ren, X., Olson, J. R., Crawford, J. H., Brune, W. H., Mao, J., Long, R. B., Chen, Z., Chen, G., Avery, M. A., Sachse, G. W., Barrick, J. D., Diskin, G. S., Huey, L. G., Fried, A., Cohen, R. C., Heikes, B., Wennberg, P. O., Singh, H. B., Blake, D. R., and Shetter, R. E.: HO_x chemistry during INTEX-A 2004: observation, model calculation, and comparison with previous studies, J. Geophys. Res., 113, D05310, doi:10.1029/2007JD009166, 2008.

Serça, D., Guenther, A., Klinger, L., Vierling, L., Harley, P., Druilhet, A., Greenberg, J., Baker, B., Baugh, W., Bouka-Biona, C., and Loemba-Ndembi, J.: EXPRESSO flux measurements at upland and lowland Congo tropical forest site, Tellus B, 53, 220–234, 2001.

Sharkey, T. D. and Yeh, S.: Isoprene emission from plants, Annu. Rev. Plant Phys., 52, 407–436, 2001.

Shim, C., Wang, Y., Choi, Y., Palmer, P. I., Abbot, D. S., and Chance, K.: Constraining global isoprene emissions with Global Ozone Monitoring Experiment (GOME) formaldehyde column measurements, J. Geophys. Res., 110, D24301, doi:10.1029/2004JD005629, 2005.

Spurr, R. J. D., Kurosu, T. P., and Chance, K. V.: A linearized discrete ordinate radiative transfer model for atmospheric remote-sensing retrieval, J. Quant. Spectrosc. Ra., 68, 689–735, 2001.

ACPD
14, 6951–6979, 2014

Stavrakou, T., Müller, J.-F., De Smedt, I., Van Roozendael, M., van der Werf, G. R., Giglio, L., and Guenther, A.: Evaluating the performance of pyrogenic and biogenic emission inventories against one decade of space-based formaldehyde columns, Atmos. Chem. Phys., 9, 1037–1060, doi:10.5194/acp-9-1037-2009, 2009a.

Stavrakou, T., Müller, J.-F., De Smedt, I., Van Roozendael, M., van der Werf, G. R., Giglio, L., and Guenther, A.: Global emissions of non-methane hydrocarbons deduced from SCIAMACHY formaldehyde columns through 2003–2006, Atmos. Chem. Phys., 9, 3663–3679, doi:10.5194/acp-9-3663-2009, 2009b.

Torres, O., Tanskanen, A., Veihelmann, B., Ahn, C., Braak, R., Bhartia, P. K., Veefkind, P., and Levelt, P.: Aerosols and surface UV products from Ozone Monitoring Instrument observations: an overview, J. Geophys. Res., 112, D24S47, doi:10.1029/2007JD008809, 2007.

Trainer, M., Williams, E. J., Parrish, D. D., Buhr, M. P., Allwine, E. J., Westberg, H. H., Fehsenfeld, F. C., and Liu, S. C.: Models and observations of the impact of natural hydrocarbons on rural ozone, Nature, 329, 705–707, 1987.

White, F.: The Vegetation of Africa – A Descriptive Memoir to Accompany the UNESCO/AETFAT/UNSO Vegetation Map of Africa, Natural Resources Research Report XX, U.N. Educational, Scientific and Cultural Organization, Paris, 356 pp., 1983.

Yang, W., Shabanov, N. V., Huang, D., Wang, W., Dickinson, R. E., Nemani, R. R., Knyazikhin, Y., and Myneni, R. B.: Analysis of leaf area index products from combination of MODIS Terra and Aqua data, Remote Sens. Environ., 104, 297–312, doi:10.1016/j.rse.2006.04.016, 2006.

ACPD
14, 6951–6979, 2014

Table 1. Isoprene emission factors for African plant functional types[a].

Plant functional type	Emission factor [mg C m^{-2} h^{-1}] MEGAN	OMI
MODIS IGBP classification[b]		
Evergreen broadleaf trees	4.3 ± 2.0	2.7 ± 1.0
Deciduous broadleaf trees	4.4 ± 1.7	2.9 ± 0.2
Woody savannas	3.2 ± 1.3	2.6 ± 1.0
Savannas	2.9 ± 1.2	2.3 ± 0.8
Shrubs	3.0 ± 1.3	1.6 ± 0.8
Grasses	1.8 ± 0.9	1.6 ± 0.9
Crops	1.4 ± 0.9	1.6 ± 0.6
Mosaic of crops and natural vegetation	2.3 ± 1.1	2.5 ± 1.0
GLC 2000 classification[c]		
Evergreen broadleaf trees	4.4 ± 1.9	2.5 ± 1.0
Deciduous broadleaf trees	3.0 ± 1.3	2.7 ± 0.9
Shrubs	3.1 ± 1.6	2.2 ± 1.0
Herbs	2.4 ± 1.3	1.9 ± 0.9
Sparse herbs or shrubs	2.4 ± 1.2	1.5 ± 0.7
Cultivated land	1.8 ± 1.1	2.2 ± 0.9
Mosaic of crops and natural vegetation	3.0 ± 1.3	2.7 ± 0.7
Mosaic of crops and shrubs or grasses	2.6 ± 1.0	1.9 ± 0.9

[a] Isoprene emission factor E_o in Eq. (1) at standard conditions of air temperature (303 K) and photosynthetically active radiation (1000 µmol photons m^{-2} s^{-1}). Values are means and standard deviations obtained by mapping the E_o data from Fig. 5 onto the MODIS IGBP and GLC 2000 land maps. Plant functional type classifications are as given by each land map.
[b] Friedl et al. (2002) and shown in Fig. 1.
[c] Mayaux et al. (2006).

ACPD
14, 6951–6979, 2014

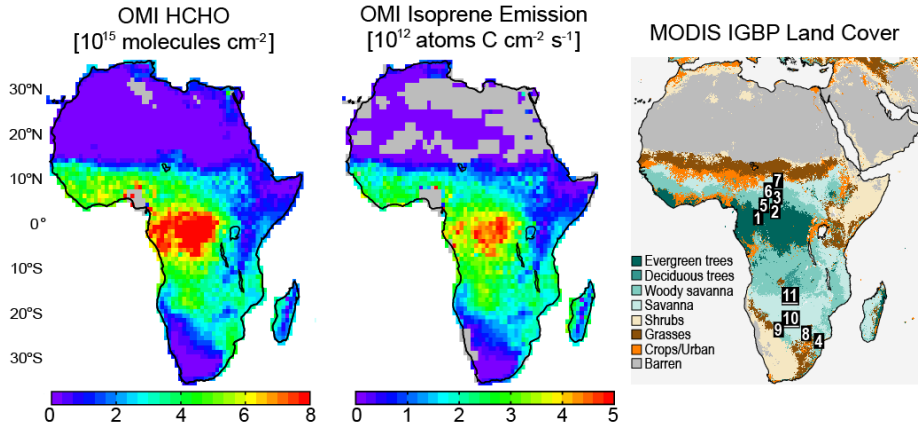

Fig. 1. Annual mean (2005–2009) OMI HCHO vertical columns at 1° × 1° horizontal resolution screened for biomass burning and anthropogenic HCHO (left), and resulting OMI-derived isoprene emissions (center), as derived by Marais et al. (2012) and summarized in the text. The OMI observations are at 13:30 LT and the OMI-derived isoprene emissions are for 12:00–15:00 LT. The right panel is a MODIS IGBP land cover map (Friedl et al., 2002) with numbers showing the location of isoprene flux measurements used to evaluate the OMI-derived isoprene emissions. These include 1. Serça et al. (2001) for March and November 1996; 2. Klinger et al. (1998) for 1995–1996 (Fig. 5) and Greenberg et al. (1999) for November–December 1996 (Fig. 2), 3. Greenberg et al. (1999) for November–December 1996, 4. Guenther et al. (1996) for December 1992 (Fig. 5) and Harley et al. (2003) for February 2001 (Fig. 2), 5–7. Klinger et al. (1998) for 1995–1996, 8–11. Otter et al. (2002) for February–March 2001.

ACPD
14, 6951–6979, 2014

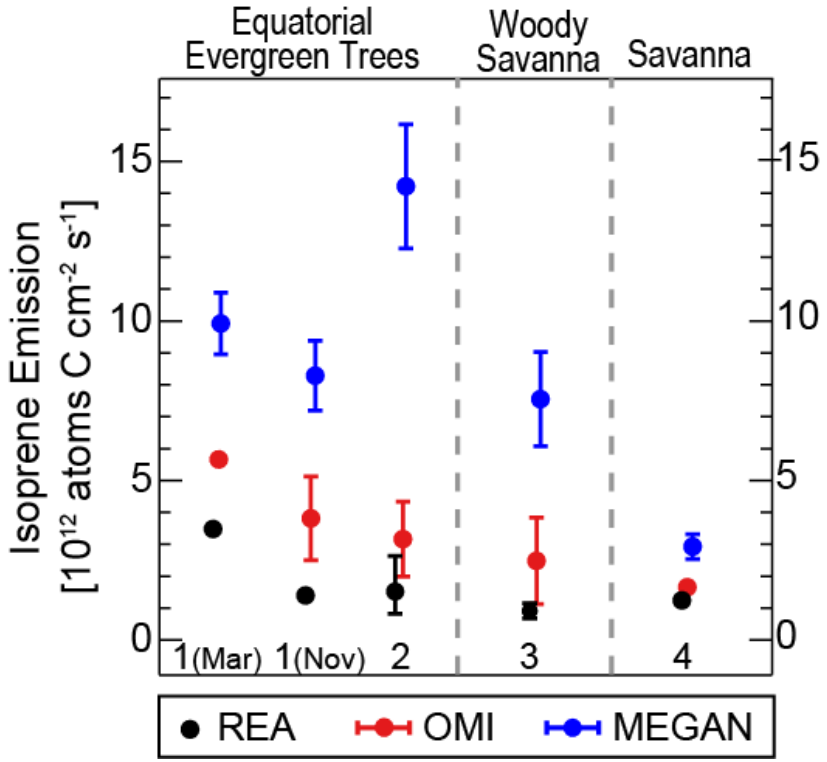

Fig. 2. Mean canopy-scale isoprene emissions at African sites 1–4 (see Fig. 1) measured by relaxed-eddy accumulation (REA), and comparison to OMI-derived and MEGAN values. All values are for 12:00–15:00 LT, with diurnal correction for REA measurements at sites 2 and 3 (see text). Vertical bars on the REA measurements for sites 2–3 are the interquartile ranges over the aircraft sampling domain given in Greenberg et al. (1999). OMI-derived and MEGAN values are 2005–2009 monthly averages for the site locations and observation times, with interannual standard deviations shown as vertical bars. Mar=March, Nov=November.

ACPD
14, 6951–6979, 2014

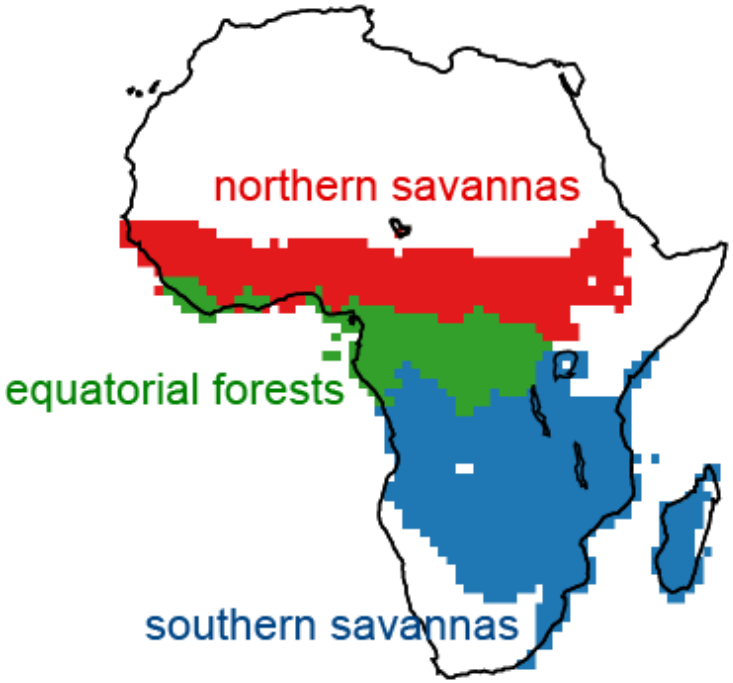

Fig. 3. Coherent regions used for analysis of the factors controlling OMI-derived isoprene emissions: equatorial forests (green), northern savannas (red), and southern savannas (blue). Land cover definitions are from the MODIS IGBP map (Fig. 1).

ACPD
14, 6951–6979, 2014

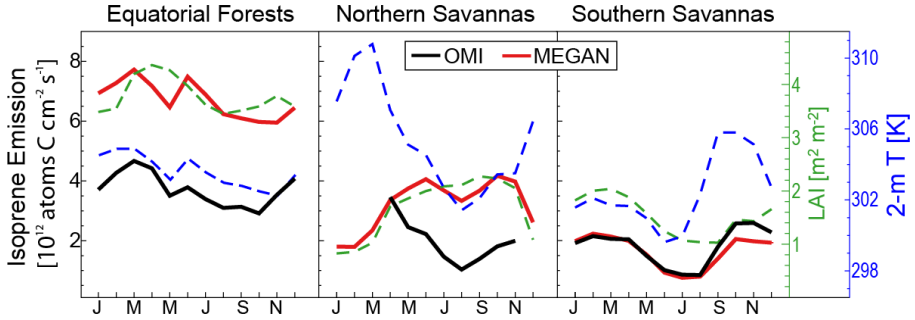

Fig. 4. Seasonality of isoprene emissions and environmental variables averaged over the coherent African regions of Fig. 3. Monthly mean OMI-derived (black) and MEGAN (red) isoprene emissions are shown together with GEOS-5 2 m temperature (blue) and MODIS LAI (green). OMI-derived isoprene emissions are not available for northern savannas in December–March because of biomass burning interference. Emissions and 2 m temperature are for 12:00–15:00 LT. LAI is the combined Terra and Aqua product (Yang et al., 2006). All data are means for 2005–2009.

ACPD
14, 6951–6979, 2014

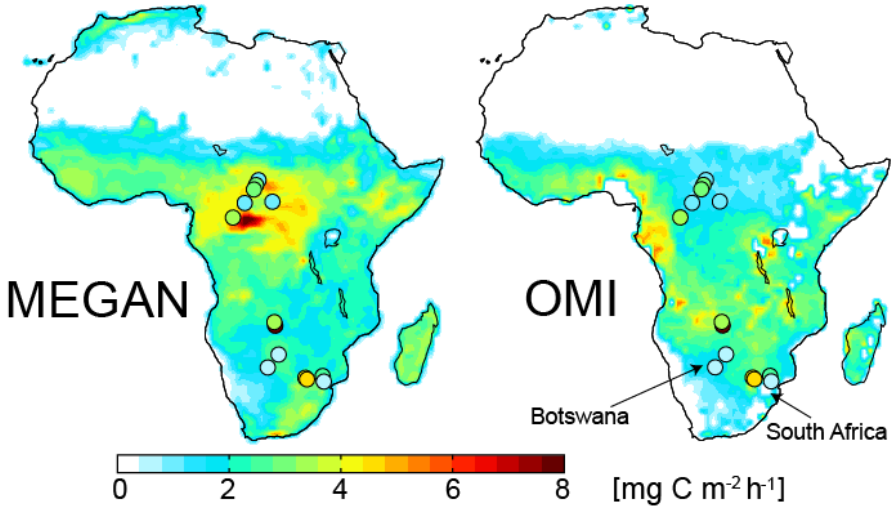

Fig. 5. Isoprene emission factors (E_o in Eq. 1) representing the emission flux under standard conditions. Measured landscape-level emission factors from field sites (circles; references given in Fig. 1) are compared to those used in MEGAN (left) and obtained with OMI (right). OMI data missing in Nigeria are due to interference from anthropogenic HCHO, and in East Africa and Namibia/South Africa due to excessive departure from standard conditions (see text for details).

ACPD
14, 6951–6979, 2014

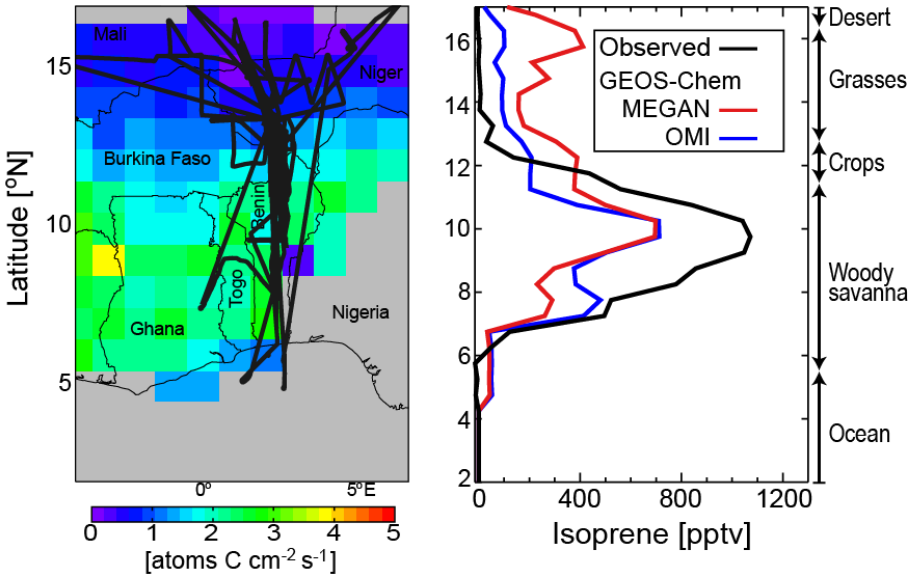

Fig. 6. Latitudinal variability of isoprene in West Africa. Left panel shows the July–August 2006 AMMA flight tracks superimposed on July–August 2005–2009 OMI-derived isoprene emissions (Marais et al., 2012). Right panel shows boundary-layer (< 1 km) isoprene concentrations along the AMMA flight tracks; observations averaged over 0.5° latitude bands are compared to GEOS-Chem model results using either MEGAN or OMI-derived isoprene emission factors E_o. Dominant MODIS IGBP biomes along the flight tracks are indicated.

ACPD
14, 6951–6979, 2014

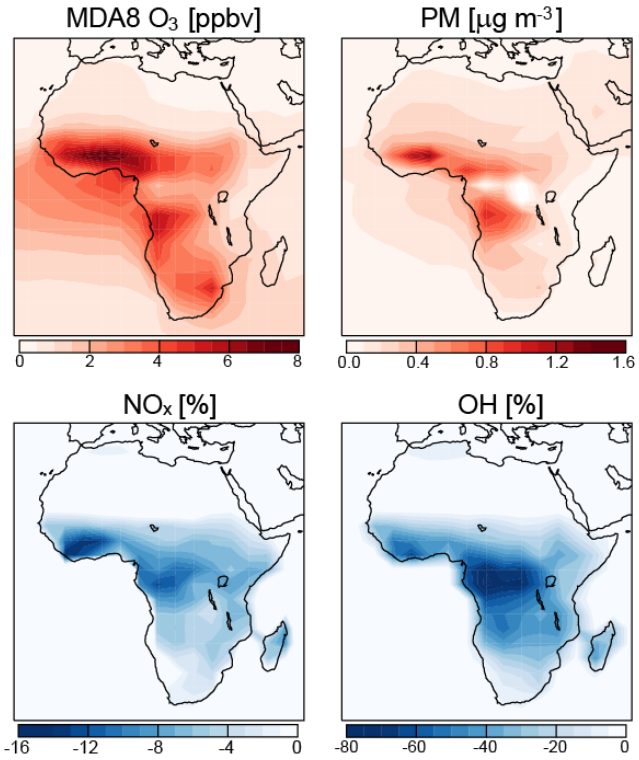

Fig. 7. Effect of African isoprene emissions on regional oxidant chemistry and particulate matter in surface air. Shown are the annual mean differences between GEOS-Chem simulations with and without African isoprene emissions for surface daily maximum 8 h average (MDA8) O_3, particulate matter (PM), NO_x, and OH. MDA8 O_3 and PM are absolute differences and NO_x and OH are relative differences. The simulation of isoprene emission uses OMI-derived emission factors.

ACPD
14, 6951–6979, 2014